BISON Fuel Fragmentation Relocation and Dispersal (FFRD) Assessment Database for Eventual Use in Bayesian Calibration

September 2023

Technical Report

Kyle A. Gamble[1]

[1]Idaho National Laboratory

Idaho National Laboratory

BISON Fuel Fragmentation Relocation and Dispersal (FFRD) Assessment Database for Eventual Use in Bayesian Calibration

Technical Report

Kyle A. Gamble[1]

[1]Idaho National Laboratory

September 2023

Idaho National Laboratory
Computational Mechanics and Materials Department
Idaho Falls, Idaho 83415

http://www.inl.gov

Page intentionally left blank

Abstract

Existing light-water reactor (LWR) fuel vendors have been interested in seeking increased discharge burnups of nuclear fuel rods for improved economics for quite a few years. With increased burnups come additional challenges that must be addressed. It has been experimentally observed that average burnups higher than the current regulatory limit of 62 MWd/kgU may undergo fuel fragmentation, relocation, and dispersal (FFRD) during a loss-of-coolant accident (LOCA). Industry must demonstrate approaches to mitigate FFRD. In an effort to support industry, the Nuclear Energy Advanced Modeling and Simulation (NEAMS) program within the U.S. Department of Energy (DOE) has for several years invested in developing multiscale models and creating a validation/assessment database for these models to study the mechanisms driving FFRD. This report provides an update on changes made to the assessment database and new models added to BISON to support the study of fuel rod behavior during FFRD. An effort has been initiated this year to begin adding dedicated inputs to the publicly available Virtual Test Bed (VTB) repository for industry use. A section of this report details the efforts made in this area. NEAMS has recently developed new capabilities in the Multiphysics Object-Oriented Simulation Environment (MOOSE) framework's stochastic tools module for calibration using Bayesian inference. The goal in the future is to use these capabilities to calibrate and identify weaknesses in the existing BISON models for FFRD. The report concludes with a discussion on the models most likely to benefit the most from such calibration.

Acknowledgment

Declaration of Competing Interest

The authors declare that they have no known competing financial interests or personal relationships that could appear to have influenced the work reported in this technical report.

Orcid

Kyle A. L. Gamble   ⓘD   0000-0002-8487-8077

Contents

List of Figures

List of Tables

Acronyms

ANL   Argonne National Laboratory

BWR   boiling water reactor

CASL   Consortium for Advanced Simulation of Light Water Reactors

DOE   U.S. Department of Energy

FFRD   fuel fragmentation, relocation, and dispersal

HBS   high-burnup structure

INL   Idaho National Laboratory

LDRD   Laboratory Directed Research and Development

LLS   lower length scale

LOCA   loss-of-coolant accident

LWR   light-water reactor

MOOSE   Multiphysics Object-Oriented Simulation Environment

NEAMS   Nuclear Energy Advanced Modeling and Simulation

NFIR   Nuclear Fuel Industry Research

NRC   Nuclear Regulatory Commission

ORNL   Oak Ridge National Laboratory

PWR   pressurized-water reactor

RIL   research information letter

SATS   Severe Accident Test Station

SCIP   Studsvik Cladding Integrity Project

tFGR   transient fission gas release

VTB   Virtual Test Bed

VVER   water-water energy reactor

1. Introduction

Over the years, the Nuclear Energy Advanced Modeling and Simulation (NEAMS) program has performed advanced modeling and simulation research in the area of fuel fragmentation, relocation, and dispersal (FFRD) during loss-of-coolant accidents (LOCAs). Much of the focus has been using lower length scale modeling to develop a more physics-based model for fuel pulverization [2, 3, 4] to be implemented into the engineering scale fuel performance code BISON [54]. Evaluation of these incremental developments to the pulverization model has been done separately using existing separate effects and integral validation cases available in BISON [22, 23]. This year's report is primarily concerned with further improvements to the existing simulations available in the validation suite including simulation refinements (e.g., power history), mesh sensitivity, and comparisons to additional measured data. To compare to additional experimental data, new models have been added, or existing models have been modified. Details of these improvements are provided in Section 2. The impact of these models on select validation cases is included in Section 3. In addition, to make inputs more accessible to industry, examples containing the recommended material and behavior models for normal operation and LOCA are in the process of been added to the Virtual Test Bed (VTB) public repository [24]. A description of these cases is provided in Section 4. Finally, the report ends with a summary of the Bayesian capabilities developed by Dhulipala et al. [13] and identifies the models available in BISON applicable to FFRD and LOCA analyses that would benefit from calibration using these new capabilities.

2. Advancements in Models for FFRD and LOCA

The task focusing on improving the assessment database in BISON includes modifications to existing models and the addition of new models as they become available. This includes improvements to models not only under FFRD but also those that apply during normal operation as well as models that depend upon the irradiation history that could impact the calculated results during a LOCA transient. Advancements or additions have been made in three areas this fiscal year: fuel dispersal, fuel and cladding elongation, and fragment and pulver shape. In the following subsections, the models are described, and regression testing is provided to demonstrate proper implementation into BISON for use in Section 3 and Section 4.

2.1   Fuel and Cladding Elongation

During normal operation, the fuel and cladding come into mechanical contact. Early validation of BISON [53] treated this mechanical interaction as frictionless allowing the fuel and cladding to slide freely past one another due to computational difficulties in resolving frictional interactions. In reality, this frictional interaction will influence the stress state during normal operation and may impact the inelastic deformation the cladding experiences. Most importantly, fuel and cladding elongation will be impacted by the inclusion of friction as the fuel will drive the axial displacement of the cladding upon mechanical contact rather than simply sliding freely. This will result in larger cladding elongation predictions when friction is included. Recent advancements in the last few years have introduced mortar-based contact methods into the underlying MOOSE framework that have significantly increased the robustness of the frictional contact algorithms for 2D-RZ axisymmetric and 3D problems.

Many of the models in BISON for FFRD currently require the use of the Layered1D [41] geometry representation of the fuel rod due to advantages of discrete layers for keeping track of axial fuel relocation. In a Layered1D simulation, the out-of-plane (axial) effects in each layer are accounted for by a single out-of-plane strain (ϵ_{yy}) for each ith layer. Until recently, frictional effects were not included in this out-of-plane strain. The details of the algorithmic implementation can be found in [44]. The impact of including friction on FFRD validation is investigated in Section 3. The algorithm is also included in the frictional versions of the VTB examples discussed in Section 4.

2.2 Fragment and Pulver Shape

The axial relocation model in BISON assumed a binary system of fuel particles termed fragments (large) and pulvers (small) to compute an effective packing fraction in layers where fuel had relocated. The effective packing fraction, ϕ, is computed by solving the following equation using an internal Newton solve:

$$a^2 + 2Gab + b^2 = 1 \tag{2.1}$$

where

$$a = \frac{\phi_p \left(\phi_f - x_f \phi \right)}{\phi \phi_f} \tag{2.2}$$

$$b = \frac{\phi_p \phi_f - \phi \phi_f \left(x_p + x_f \phi_p \right)}{\phi \phi_p \left(1 - \phi_f \right)} \tag{2.3}$$

and G is a parameter that depends upon the difference in shape between the fragments and pulver, x_p is the pulver mass fraction, and x_f is the fragment mass fraction given by $1 - x_p$. In the preceding equations, ϕ_f and ϕ_p represent the packing fraction if the crumbled bed of fuel particles was entirely made up of fragments or pulvers, respectively. Jernkvist and Massih suggest values of $\phi_f = 0.69$ and $\phi_p = 0.72$. The G parameter is calculated by:

$$G = \begin{cases} 0.738 \left(D_p^p / D_p^f \right)^{-1.566}, & D_p^p / D_p^f \leq 0.824 \\ 1, & D_p^p / D_p^f > 0.824 \end{cases} \tag{2.4}$$

where D_p^p and D_p^f are the equivalent packing diameters of the pulvers and fragments. The equivalent packing diameter is determined via:

$$D_p = \left(3.9431 - \frac{4.5684}{\psi} + \frac{1.8660}{\psi^2} \right) V_p^{1/3} \tag{2.5}$$

where ψ is the sphericity of the particle, and V_p is the volume of the particle. Since its initial implementation in BISON, the computation of the effective packing fraction has assumed the shape of fragments, and pulvers are prismatic triangular prisms and octahedrons, respectively. A prismatic triangular prism has the same axial height as the characteristic side length of the triangle. This results in $\psi = 0.716$ and $V_p = 0.4330 l_f^3$ for fragments and $\psi = 0.846$ and $V_p = 0.4714 l_p^3$ for pulvers. By default l_p, the characteristic length of the pulver is taken as 100 μm, and l_f, the characteristic length of the fragment is computed by:
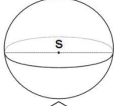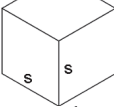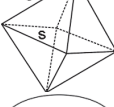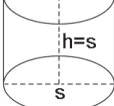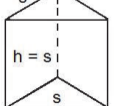
$$l_f = D_{FP} \min \left(1.0, \frac{\pi}{n_f} \right) \tag{2.6}$$

where D_{FP} is the fuel pellet diameter, and n_f is the number of fragments formed due to cracking under thermal gradients. BISON contains three models for computing n_f: BARANI [7], COINDREAU [12],

and WALTON [52]. The details for these models can be found on the BISON documentation page [38] or in their respective references. In all cases, the number of fragments is a function of the peak power observed. For the COINDREAU [12] and WALTON [52], a burnup dependence is also introduced resulting in more cracking and irradiation progresses.

It is evident from experimental observations that multiple fragment shapes and sizes are observed. To enable sensitivity analysis on the binary system of particles in the axial relocation algorithm, options for various particle shapes as described in Jernkvist and Massih [27] have been added as user definable options. The default values still remain as triangular prisms and octahedrons of fragments and pulvers. Table 2.1 identifies the assumed particle shapes and provides the sphericity and volume of a particle for that shape. In the table, s is the characteristic length, and therefore, $s = l_f$ for fragments and $s = l_p$ for pulvers.

Table 2.1. Sphericity and volume of fuel particles with given shapes and characteristic dimensions. Schematics in the second column reproduced from [27].

Shape and Dimension		ψ (-)	V_p (m^3)
Sphere with diameter s		1.000	$0.5236s^3$
Cube with side s		0.806	s^3
Octahedron with side s		0.846	$0.4714s^3$
Ideal cylinder, $h = s$		0.874	$0.7854s^3$
Triangular prism s, $h = s$		0.716	$0.4330s^3$

The existing BISON regression test for computation of the effective packing fraction using the default particle shapes was extended to test all combinations of potential particle shapes. The test is designed such that $x_p = 0.51$. The maximum power supplied to the fuel was 15 kW/m, and the pellet average burnup was 66.66 MWd/kgU. The power and average burnup are used to determine n_f by the three different fragmentation correlations. Table 2.2 presents the results of the test for all combinations of fragmentation models and particle shape computed by BISON which have been independently verified by hand calculations. The fragment effective diameter, D_p^f, pulver

effective diameter, D_p^p, and the effective packing fraction, ϕ, are shown. A few key observations can be seen from the results. The first is selecting the particle shape does not influence the effective packing fraction by a significant amount, and the second is the `COINDREAU` fragmentation model results in a consistently lower effective packing fraction than `BARANI` or `WALTON`. However, the choice of fragmentation model greatly impacts the fragment effective diameter, which may impact fuel dispersal calculations.

Table 2.2. Computed effective packing fractions and equivalent fragment diameters for the test case for each of the large scale fragmentation models and all shape combinations. The default shape combination row is highlighted in yellow. The default large fragment shape correlation is highlighted blue.

Fragment Shape	Pulver Shape	D_p^f (mm) BARANI	ϕ BARANI	D_p^f (mm) COINDREAU	ϕ COINDREAU	D_p^f (mm) WALTON	ϕ WALTON	D_p^p (mm)
Sphere	Sphere	5.4717	0.83349	1.7671	0.82877	2.5959	0.83132	0.1
Sphere	Cube	5.4717	0.83326	1.7671	0.82745	2.5959	0.83057	0.11475
Sphere	Octahedron	5.4717	0.83365	1.7671	0.82966	2.5959	0.83182	0.08952
Sphere	Cylinder	5.4717	0.83338	1.7671	0.82816	2.5959	0.83098	0.10692
Sphere	Tri. Prism	5.4717	0.83363	1.7671	0.82954	2.5959	0.83175	0.090975
Cube	Sphere	6.2787	0.83369	2.0278	0.82986	2.9788	0.83193	0.1
Cube	Cube	6.2787	0.83349	2.0278	0.82877	2.9788	0.83132	0.11475
Cube	Octahedron	6.2787	0.83381	2.0278	0.83058	2.9788	0.83233	0.08952
Cube	Cylinder	6.2787	0.83360	2.0278	0.82936	2.9788	0.83165	0.10692
Cube	Tri. Prism	6.2787	0.83380	2.0278	0.83048	2.9788	0.83228	0.090975
Octahedron	Sphere	4.8984	0.83331	1.5820	0.82773	2.3239	0.83073	0.1
Octahedron	Cube	4.8984	0.83302	1.5820	0.82617	2.3239	0.82985	0.11475
Octahedron	Octahedron	4.8984	0.83349	1.5820	0.82877	2.3239	0.83132	0.08952
Octahedron	Cylinder	4.8984	0.83318	1.5820	0.82701	2.3239	0.83032	0.10692
Octahedron	Tri. Prism	4.8984	0.83347	1.5820	0.82863	2.3239	0.83124	0.090975
Cylinder	Sphere	5.8506	0.83359	1.8895	0.82933	2.7757	0.83163	0.1
Cylinder	Cube	5.8506	0.83338	1.8895	0.82813	2.7757	0.83096	0.11475
Cylinder	Octahedron	5.8506	0.83374	1.8895	0.83013	2.7757	0.83208	0.08952
Cylinder	Cylinder	5.8506	0.83349	1.8895	0.82877	2.7757	0.83132	0.10692
Cylinder	Tri. Prism	5.8506	0.83372	1.8895	0.83002	2.7757	0.83202	0.090975
Tri. Prism	Sphere	4.9779	0.83334	1.6077	0.82789	2.3616	0.83082	0.1
Tri. Prism	Cube	4.9779	0.83306	1.6077	0.82637	2.3616	0.82996	0.11475
Tri. Prism	Octahedron	4.9779	0.83352	1.6077	0.82891	2.3616	0.83140	0.08952
Tri. Prism	Cylinder	4.9779	0.83321	1.6077	0.82719	2.3616	0.83043	0.10692
Tri. Prism	Tri. Prism	4.9779	0.83349	1.6077	0.82877	2.3616	0.83132	0.090975

2.3   Fuel Dispersal

One of the earliest models for fuel dispersal estimates was to assume that all fuel <1 mm in size anywhere within the fuel rod may be dispersed [43]. The research information letter (RIL) published by the NRC proposed six additional models for determining the amount of fuel dispersed in a fuel performance analysis. It should be mentioned that RIL is not regulatory guidance but may be used to determine whether any regulatory actions are necessary. The six proposed models are outlined below:

1. All fuel smaller than 1 mm in the length of the rod with greater than 3% hoop strain

2. All fuel smaller than 2 mm in the length of the rod with greater than 3% hoop strain
3. All fuel in the length of the rod with greater than 3% hoop strain
4. All fuel smaller than 1 mm in the length of the rod with greater than 2% hoop strain
5. All fuel smaller than 2 mm in the length of the rod with greater than 2% hoop strain
6. All fuel in the length of the rod with greater than 2% strain

where these models only apply to regions of the fuel with an average burnup >55 MWd/kgU.

The authors presented comparisons to data from Studsvik Cladding Integrity Project (SCIP) test series. The program began in 2004 and is currently in its fourth iteration (i.e., SCIP-IV). The RIL only shows comparisons of the six proposed models for fuel dispersal against the experimental measurements for dispersal but not enough detail is provided to enable simulations of these experiments. The authors of the RIL [6] also make a clear distinction between dispersed and mobile fuel. The definitions are as follows:

Dispersed fuel: Fuel that was dispersed during the experiment.

Mobile fuel: Fuel that could relocate even if relocation did not occur during the experiment. Often determined by measuring the amount of additional fuel dispersed after shaking of the experimental apparatus. Therefore, mobile fuel encompasses that dispersed during the transient and after shaking.

It is suggested when selecting a dispersal model that comparisons to experiments be made against the mobile fuel measurements if available. This is because the models do not account for rupture opening size or the volume and pressure evolution of the fill gas during the transient. The authors of the RIL state that it is reasonable to assume that above 55 MWd/kgU any fuel within the length of the rod greater than 3% cladding strain could disperse. This suggests that the third proposed model is considered to be reasonably conservative.

Regression testing and documentation for the RIL dispersal model have been added to BISON. The model couples to the existing axial relocation algorithm in BISON to obtain the fuel particle size to determine if material has been dispersed. Therefore, the Layered1D formulation in BISON must be used. In the test, a 0.5 m rodlet is represented by 5 axial layers. In the Layered1D formulation, the physical location of the layers is at the mid-height associated with the layer. Therefore the axial locations in which the dispersal calculation is evaluated are 0.05 m, 0.15 m, 0.25 m, 0.35 m, and 0.45 m. The fuel pellet has an outer radius of 4.5 mm, which gives an initial fuel volume of 31.8086 cm^3. The fragment and pulver equivalent diameters are assumed to be 1.6 mm and 0.1 mm, respectively. A displacement is applied to the inner surface of the cladding given by:

$$\Delta R_{ci} = 2 \times 10^{-5} t \sin\left(\frac{\pi y}{0.5}\right) \tag{2.7}$$

where y is the axial position, and t is the time in seconds. The duration of the simulation is 28 seconds. Figure 2.1 illustrates the evolution of the calculated fuel dispersal as a function of time as the hoop strain evolves for the six dispersal options. The 2 mm and all fuel particle sizes have the same dispersal profiles as expected given the equivalent diameters of the particles assumed. Dispersal values at early times correspond to fuel in the central region of the rodlet due to the

6

symmetric nature of the displacement profile. The axial positions of the top and bottom layers at 0.05 m and 0.45 m result in complete fuel dispersal for all cases with all or 2mm particle size as the hoop strain exceeds 3% even at these locations.
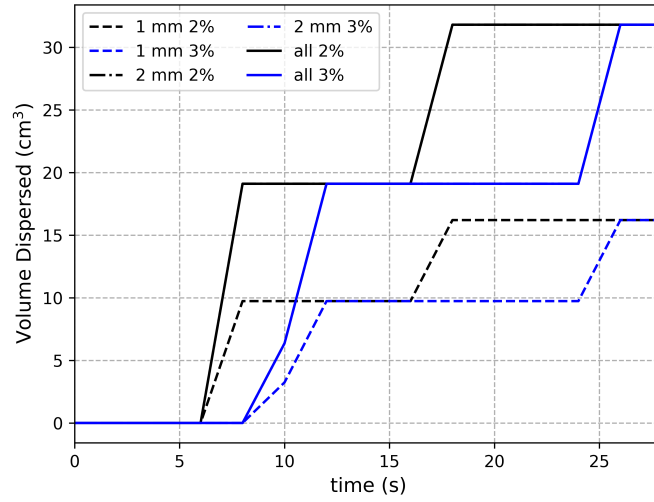
Figure 2.1. Volume of fuel dispersed as a function of time.

3. Assessment Database

The models available in BISON must be assessed against experimental data. Over the years NEAMS, Consortium for Advanced Simulation of Light Water Reactors (CASL), and Laboratory Directed Research and Development (LDRD) funding, various validation or assessment cases have been added to BISON. Cases assessing phenomena related to LOCA and FFRD began in about 2015. As new empirical or LLS-informed capabilities are added, the existing cases are updated and rerun to evaluate the impact on experiments. In some cases, sensitivity analyses are also completed to evaluate the impact of model options that can be set by the user. BISON's full assessment suite, including those as part of the FFRD validation, is run nightly to evaluate the impact of day-to-day changes on the gold standard results. Any changes to the expected results are carefully evaluated to determine if the changes are expected, and if so, the gold standards are updated.

3.1 Existing Assessment Cases in BISON

Table 3.1 presents the currently available cases in BISON that have experimental data to compare model predictions for LOCA and FFRD phenomena. An 'X' is used to indicate whether an experiment has measured data for the identified quantity of interest. It should be noted that currently BISON results are not compared to every quantity measured in the experiments. In some cases, the simulation setup needs to be modified to elucidate reasonable insight into some measured quantities (e.g., HBS thickness, see Section 3.4.3).

   The IFA-650 test series was completed at the Halden reactor in Norway [16, 30, 15, 31, 49, 46] and consisted of 15 experiments. The experiments were all conducted on pre-irradiated fuel rods, except IFA-650.2 which was fresh, with varying levels of burnup. The primary goal was to investigate the severity of fuel fragmentation, relocation, and dispersal as functions of burnup for pressurized-water reactor (PWR), boiling water reactor (BWR), and water-water energy reactor (VVER) reactor conditions. In particular, IFA-650.9 and IFA-650.14 were interesting. IFA-650.9 had a double cladding balloon with only one rupture and severe fuel relocation. IFA-650.14 was designed to have large cladding strain without rupture. IFA-650 rods 2, 4, 9, 10, and 14 have been analyzed with BISON.

   The Nuclear Regulatory Commission (NRC)-sponsored Studsvik [26, 46, 18] test series consisted of two separate sets of experiments. The first four (189, 191, 192, and 193) were conducted on high-burnup PWR fuel segments all with ∼70 MWd/kgU discharge burnup. The differences between the rods consisted of the initial refabrication pressure, desired peak cladding temperature, or hold at the

peak cladding temperature prior to quenching. These rods all experienced large rupture openings and significant fuel dispersal. The remaining two experiments (196 and 198) were conducted on pre-irradiated fuel segments with a much lower discharge burnup 55 MWd/kgU. These rods had much smaller rupture openings than the high-burnup rods, and no fuel was dispersed during the experiments. Fuel relocation did occur as the missing length of the rodlets was significant. To date, BISON has been used to analyze rods 191, 192, and 193 from this test series.

The remaining cases available in BISON come from test series on cladding-only tubes to evaluate the Erbacher high-temperature creep model [17] with a focus on time to rupture, rupture temperature, rupture pressure, and cladding distention (i.e., maximum strain). These experiments are commonly referred to as separate effects tests. The PUZRY [40] cases were conducted on fresh cladding tubes that were exposed to a constant isothermal temperature in the range of 700–1200 °C and the internal pressure ramped until rupture. The ramping rates ranged from 0.005–0.263 bar/s. The Oak Ridge National Laboratory (ORNL) tests [36] were completed in the Severe Accident Test Station (SATS) [45] facility. Both standard Zircaloy tubes (both Zircaloy-2 and Zircaloy-4) and advanced FeCrAl tubes were tested. The internal pressure was held relatively constant, and the temperature was ramped up at 5 K/s up to 1473 K followed by a hold and quench. Cladding rupture occurs during the temperature ramp, and the BISON simulations are terminated at rupture. The Argonne National Laboratory (ANL) tests are similar to the ORNL tests as they were conducted in the precursor facility to the ORNL SATS [9]. The REBEKA test series [17, 35] was conducted to investigate the effect of ramping rate (1 K/s to 30 K/s) on the ballooning and rupture behavior in an oxidizing environment. The internal pressure was held constant. The Hardy Tube tests [25] were conducted to look at a high ramping rates (25 K/s to 100 K/s). The initial internal pressures varied from 0.3 to 13.8 MPa. Finally, the QUENCH LOCA [47] experimental program was conducted on fuel bundles with multiple rods being subjected LOCA conditions at the same time. The primary focus was the impact of hydrogen concentration on ballooning and rupture behavior. In BISON, two rods were been analyzed from the reference bundle QUENCH-L1.

Table 3.1. Assessment cases available in BISON related to LOCA or FFRD with identified experiment measurements available for comparison. An 'X' is used to indicate whether an experiment has measured data for the identified quantity of interest.

| Test ID | IFA-650 | | | | | Studsvik | | | | PUZRY | ORNL | ANL | REBEKA | Hardy Tube | QUENCH-L1. |
Rod ID	2	4	9	10	14	191	192	193	196	31 Rods	3 Rods	3 Rods	20 Rods	16 Rods	2 Rods
Rupture Time	X	X	X	X	X	X	X	X	X	X	X	X	X	X	X
Rupture Temperature	X	X	X	X	X	X	X	X	X	X	X	X	X	X	X
Rupture Dimensions						X	X	X	X		X				X
Fragment Size Distribution	X	X	X	X	X	X	X	X	X						
Mass Fuel Dispersed	X	X	X	X	X	X	X	X	X						
HBS Thickness	X	X	X	X	X	X		X							
Axial Fuel Relocation	X	X	X	X	X										
Cladding Profilometry	X	X	X	X	X										X
Rod Internal Pressure	X	X	X	X	X	X	X	X	X	X	X	X	X	X	
Cladding Elongation†	X	X	X	X	X					X	X	X	X		
Cladding Temperature‡	X	X	X	X	X	X	X	X	X	X	X	X	X	X	X
Missing Length	X	X	X	X	X	X	X	X	X						
Maximum Burst Strain	X	X	X	X	X	X	X	X	X	X	X	X	X	X	X

† Inferred from gamma scans
‡ Prescribed directly in furnace test experiments.

3.2 Available Experiments

Many experiments have been added to the BISON assessment database for FFRD and LOCA analysis, but there is a wealth of additional experiments available to further build the assessment data. First, the remaining experiments from the IFA-650 test series could be added to the BISON assessment suite. Unfortunately, a handful of the remaining rods were VVERs in which the United States does not have interest in analyzing. A select few of the cases, IFA-650.3 and IFA-650.5, are being added in support of another project on axial gas transport. Once available, these cases can be used for studying model developments in support of the NEAMS program. The experimental data for these rods could also be used in Bayesian calibration of various models in BISON for FFRD (see Section 5). The remaining two Studsvik rods (rods 189 and 198) are also available for inclusion.

The SCIP program contains four phases dating back to 2004 each with a wealth of experimental data on cladding properties, fuel rod failure, fuel fragmentation, and transient fission gas release. These experiments are said to be well characterized and contain data used in the development of the dispersal models added to BISON. While currently access to this data is not available for the developers of BISON, progress through other programs has been made to gain access to at least the ongoing SCIP-IV data.

Over the last few years, experiments have been conducted on commercially irradiated fuel segments at the SATS facility [55]. While the tests themselves are well characterized, all that is usually known about the commercial specimen prior to the test is the discharge burnup and initial dimensions. Unfortunately, without the power history the rods were subjected to prior to the test, it becomes more difficult to develop a simulation that has the proper initial conditions prior to the experiment.

The existing BISON validation suite for normal operational cases also consists of a handful of irradiations that go to high discharge burnup (IFA-515.10, HBEP, IFA-597.3) [53]. While the focus was not on FFRD, these higher discharge burnups should include HBS formation models and account for the impact of the HBS on thermal conductivity and fission gas release. These validation cases could be included to assess the validity of the HBS models being developed as they impact measurements of interest in those experiments. These data would provide additional data points for Bayesian calibration of the HBS models.

Turnbull and the Nuclear Fuel Industry Research (NFIR) [50] program have a wealth of data on fuel fragmentation at high burnup, which was used to develop the empirical criteria for pulverization available in BISON. An attempt to obtain details on the experiments used in the derivation of the pulverization criterion was made such that the data could be used in Bayesian calibration to develop a new LLS-informed model for fuel pulverization. The data, being generated as part of the NFIR projects, require participation in NFIR to obtain access. Much like SCIP, members of the BISON and NEAMS LLS teams are not members of NFIR and therefore do not have access.

3.3 Missing Data Needs

The current assessment database contains a lot of experiments that have measurements of select key parameters as identified in Table 3.1. It is not entirely clear how these experiments map to

commercial operation since the tested specimens are usually several tens of centimeters in length, and full length rods are 4 m long. It could be argued these specimens are representative of the distances between spacer grids and therefore would be applicable. Nevertheless, full length fuel rod data would be required to confirm the impact of spacer grids FFRD during LOCA. Moreover, these experiments are generally conducted on isolated fuel rods with maximum burst trains in the range of 25 % to 100%. These sizes of balloons may not be possible in a fuel assembly where adjacent rods are also ballooning. Experimental data on rod-to-rod interactions during a LOCA would be of interest to help validated cladding deformation models. Last, of the experiments currently in BISON, only the Hardy Tube tests have temperature ramping rates >30 K/s. It has been postulated that during high-temperature ramp rates up to 100 K/s that fuel rod failure may occur due to plasticity effects long before high-temperature creep would activate. Failures early in the LOCA process would result in a more coolable geometry than those that balloon significantly leading to potential coolant channel blockage. Uncertainties on experimental measurements are also lacking for much of the available experiments from the literature.

3.4 Improvements to Existing Cases

Application of a new LLS-informed pulverization criteria has been a subject of interest for the past few years regarding FFRD validation. This model was compared to the empirical [50] pulverization threshold on the impact of fuel relocation predictions (IFA-650.4 and IFA-650.9) and fuel dispersal, assuming only pulverized fuel was dispersed (Studsvik). It was found that the physics-based model predicted no pulverization under the conditions of the experiment [23]. Therefore, the focus this year was looking into modeling assumptions and their impact on predictions. Section 2 described the addition of a new dispersal model and the ability to select the shape of particles that relocate. This section of the report documents the improvements to inputs, boundary conditions, and the addition of new models on simulations predictions.

3.4.1 Power History and Boundary Conditions

Studsvik Rods 192 and 193 were added to the assessment suite last year [23]. Assumptions were made based upon the Rod ID information available in [18] that Rod 193 being in the same assembly as Rod 191 that the base irradiation was the same, but Rod 192 base irradiation was unknown. At the time, a constant power to achieve the discharge burnup of ∼72 MWd/kgU was used. According to Flanagan et al. [19], the base irradiation power history for Rod 192 is also the same as Rod 191. This has been updated in the BISON setup of the case for Rod 192. In addition, for some of the rods, the hold time at the peak cladding temperature was off from that specified by Flanagan et al. [18]. While this change can impact simulations results during the transient due to longer term exposure at high temperature, BISON simulations are usually terminated at rupture, which occurs prior to reaching the peak temperature. Nevertheless, the corrected temperature profiles have been added to BISON such that they are available if one chooses to simulate post rupture. The updated temperature profiles for Rods 191, 192, 193, and 196 are presented in Figure 3.1. It should be noted that Rod 196 was a ramp to failure test, which will occur during the power ramp

up. The hold times for Rod 191, 192, and 193 are 5, 25, and 85 seconds, respectively.
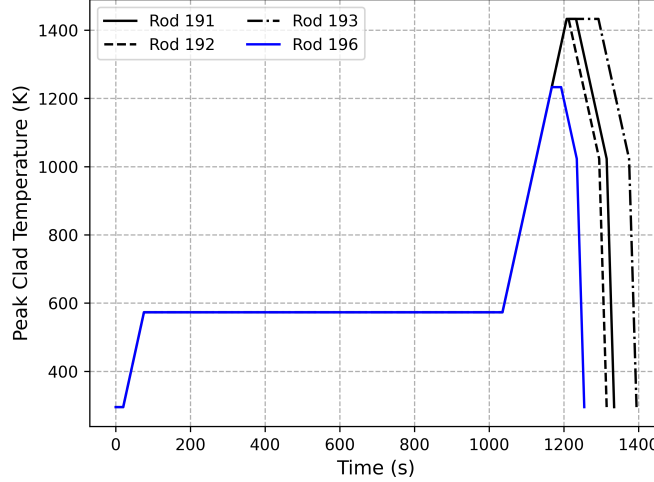

Figure 3.1. Peak cladding temperature evolution for the Studsvik rods.

3.4.2 Application of the New Dispersal Model

The newly added dispersal model requires the use of the Layered1D formulation. Of all integral tests available in BISON for FFRD, only IFA-650.4 and IFA-650.9 were developed using the Layered1D geometric representation as they were the first experiments added for which axial fuel relocation data was available. Originally, only comparisons to the total amount of fuel pulverized for the Studsvik rods was completed, as that was the earlier simplistic measure of fuel dispersal in BISON. This approach would only consider fuel at the pellet periphery as susceptible to release and ignore the possibility of larger fuel fragments in the ballooned region from also dispersing.

To apply the new dispersal model to the Studsvik rods, Layered1D version had to be created. Prior to performing sensitivity on the selected option for fuel dispersal, it was confirmed that the Layered1D and existing 2D-RZ axisymmetric simulations give the same results. Figure 3.2 presents the comparisons of key fuel performance parameters for the base irradiation of Studsvik Rod 191. For the most part, comparisons are identical. Minor deviations in fission gas release and plenum pressure are observed. Since the rodlet is refabricated prior to the transient, these small differences will not impact the behavior during the LOCA.

Using the converted Rod 191 case 6, different simulations are simulated using both the Turnbull pulverization threshold [50] and the LLS-informed model implemented last year from Aagesen et al. [4]. Recall that Gamble et al. [23] found that the LLS-informed model predicted no fuel release for Studsvik Rod 191 because no pulverization was predicted. The purpose of this study using the new dispersal model is to show irrespective of the prediction of pulverized fuel, which has a smaller size, that dispersal is expected for cases in which cladding particle size is ignored. These results are tabulated in Table 3.2.

x

13
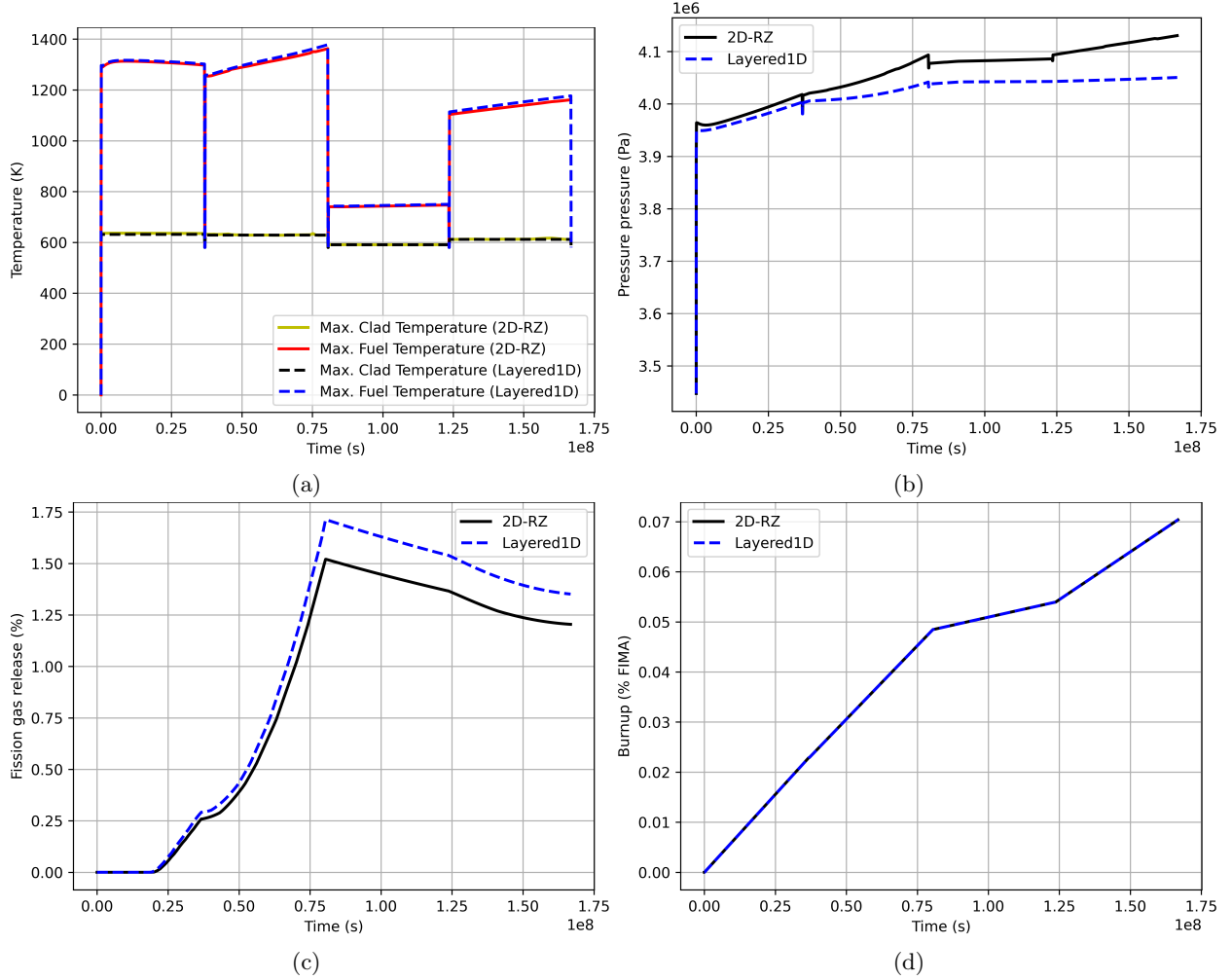
Figure 3.2. Results of the 2D-RZ to Layered1D comparison for Studsvik Rod 191, (a) maximum fuel and cladding temperatures, (b) plenum pressure, (c) fission gas release, (d) rod average burnup.

3.4.3 Mesh Refinement Studies for HBS Thickness Predictions

Williamson et al. [53] performed a radial mesh sensitivity to identify the optimal number of elements through the radius of fuel rods for BISON simulations during normal operation. Thus far, for integral LOCA analysis, this radial mesh density has been adopted. The mesh typically consists of 11 quadratic elements radial that are equally sized. In general, this mesh density is sufficient for computing temperature behavior, rod internal pressures, and other traditional metrics of interest. However, when looking at specific model behavior, this mesh may be insufficient. In an effort to explore the validation of models traditionally validated indirectly such as the HBS formation model, additional experimental data have been sought. A micrograph for the HBS thickness for Studsvik Rod 192 is reproduced from Flanagan et al. [19] in Figure 3.3. From the micrograph,

14

Table 3.2. Computed fuel dispersal using the new dispersal model for Studsvik Rod 191 for both the empirical and LLS-informed pulverization thresholds.

Dispersal Model	Mass Released LLS (g)	Mass Released Empirical (g)
< 1 mm, 2% strain	0	0.73
< 2 mm, 2% strain	0	0.73
All mm, 2% strain	14.6	14.6
< 1 mm, 3% strain	0	0.73
< 2 mm, 3% strain	0	0.73
All mm, 3% strain	14.6	14.6

the HBS thickness is estimated to be ~200 μm. Given the standard fuel radius of 4.1 mm and 11 elements, the individual resolution is 0.372 mm (372 μm). Since the HBS thickness is computed at the quadrature points, a material property in BISON, output for visualization results in an elemental average value. An element average value greater than 0.5 is deemed to be part of the HBS in the BISON simulations. Clearly, a more refined mesh is necessary to accurately compute this thickness.
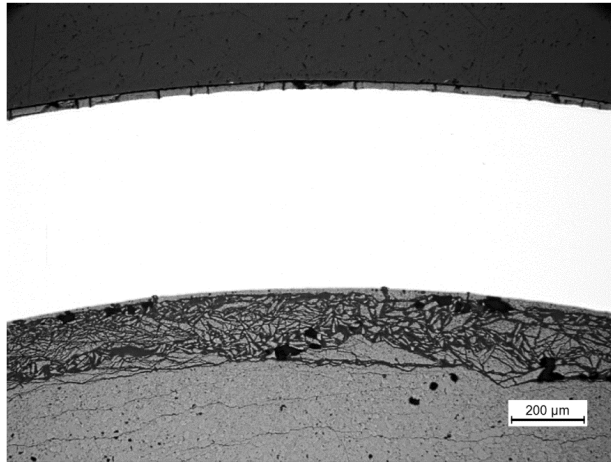
Figure 3.3. Micrograph of the fuel periphery for Studsvik Rod 192 [19].

Five different meshes were analyzed. The first was the standard mesh. Two additional meshes with the same number of radial elements employing fractional biasing factors of 0.6 and 0.8, respectively, were analyzed. These factors indicate what percentage of the previous element's radial edge length is used for the current elements' radial edge length. The final two meshes were simple doubling and quadrupling of the mesh in the radial direction from 11 to 22 and 44, respectively. A corresponding refinement in the axial direction was required to maintain reasonable aspect ratios for the elements. Figure 3.4 presents a close up of the pellet periphery region for the five different

meshes illustrating the high-burnup volume fraction. Table 3.3 reports the estimated thickness of the HBS from the contours.

Table 3.3. HBS thickness for various meshes.

	Standard	0.8 Bias Factor	0.6 Bias Factor	Double	Quadrapule
HBS Thickness (μm)	378	221	181	190	190

Figure 3.4. HBS volume fraction contours for the (a) standard, (b) 0.8 bias, (c) 0.6 bias, (d) doubly refined, and (e) quadruply refined meshes.

17

4. LWR VTB Examples

The VTB is a public repository for storing example input files for NEAMS tools [24]. Originally, the repository was designed to provide input files for several challenge problems for advanced reactor concepts. The inputs are accompanied by background information on the reactor design as well as documentation of the models used in the input. In this vein, BISON inputs would be suppor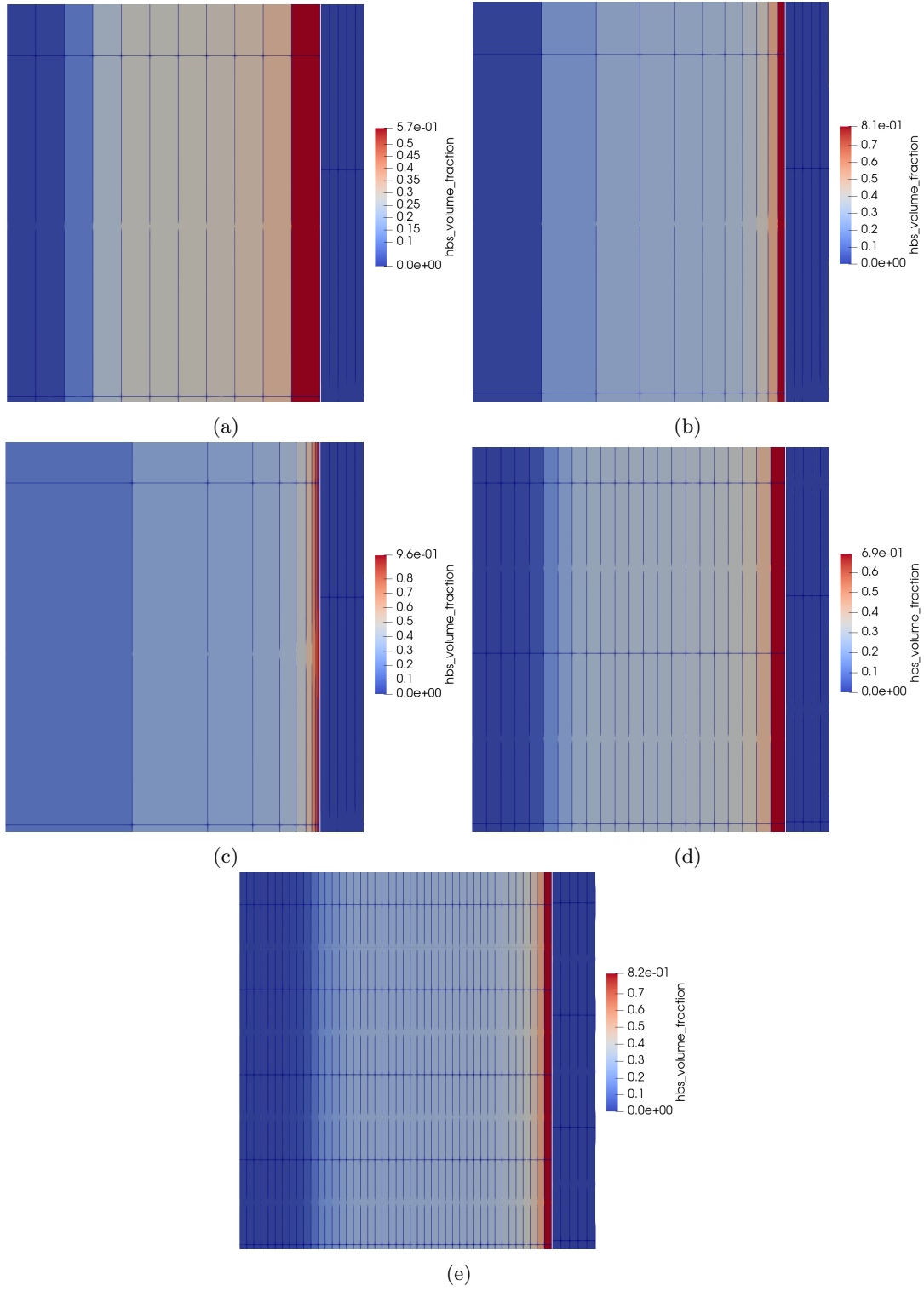ting larger multiphysics representations of the reactors. It has been decided to include examples for conventional LWR fuel rods for normal operating and accident conditions using the recommended validated models available in BISON. This also includes developing examples for accident tolerant fuel concepts. Here, a summary is provided for the normal operation to high burnup followed by a LOCA transient for PWR fuel. It should be mentioned that additional examples with comparisons to experimental data are available to interested parties on the BISON documentation website under verification and validation. Given that the VTB was originally developed for advanced reactor concepts, a new directory for LWR will be required. Subdirectories will be added for the PWR cases discussed here and for BWR to prepare for the development and inclusion of future cases that demonstrate BWR analysis with BISON.

4.1   Case Descriptions

Two cases are in the process of being added to the VTB for high-burnup applications using BISON: (1) normal operation until a rod average burnup of approximately 65 MWd/kgU is obtained and (2) a follow-on LOCA-like analysis until cladding rupture. Some of the LOCA models in BISON inherently require the Layered1D (1.5D) geometric representation, and therefore, these cases are formulated using that geometry. In a Layered1D simulation, the fuel rod is discretized into discrete axial layers that are solved independently in the radial direction with axial (out-of-plane) effects captured using a generalized plane strain approach. The simulations consider a full length fuel rod with an active fuel length of 3.658 m, a plenum height of 0.29 m, a fuel diameter of 8.2 mm, a fuel-to-clad radial gap thickness of 80 μm, and a cladding thickness of 0.56 mm. Forty axial layers are used for the active fuel region with a single layer accounting for the plenum. Sixteen EDGE3 elements are used radially through the fuel and four in the cladding. For each case (normal and LOCA-like), two simulations are planned, one including the new Layered1D friction capabilities [44] and one without.

The initial condition of fuel is representative of standard PWR UO$_2$ with a density of 95% theoretical, 5% porosity, 5% enrichment, and a grain size of 10 μm. The cladding is assumed to

be Zircaloy-4. For the thermal-hydraulic boundary condition, the BISON internal coolant channel model is used with an inlet temperature of 580 K, mass flow rate of 3800 kg/s, and inlet pressure of 15.5 MPa. The pitch between adjacent rods is assumed to be 0.0126 m.

To achieve 65 MWd/kgU, the power is increased over 1 day to 25 kW/m and held until the desired burnup is achieved. An axial profile as shown in Figure 4.1 is applied for the duration of the base irradiation case.
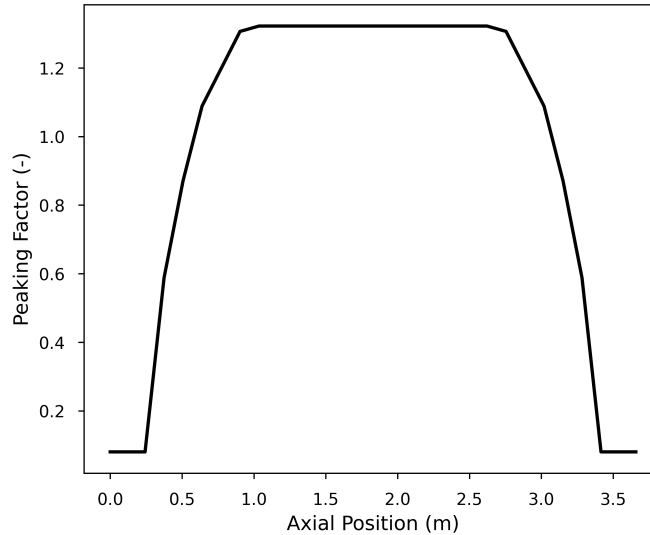
Figure 4.1. Axial power peaking profile supplied to the fuel during the normal operating VTB example.

The LOCA-like transient is reminiscent of furnace tests on small fueled specimens such as those completed at Studsvik [26] and the SATS at ORNL [45]. Typically, these furnace tests have the peak cladding temperature at the axial center of the rod, and due to the nature of the furnace, the ends are at a lower temperature. This temperature gradient is what induces localized ballooning. The evolution of the peak cladding temperature in this LOCA-like example is illustrated in Figure 4.2a, and the axial profile of the temperature once the peak reaches 1200 K is shown in Figure 4.2b. An axial temperature profile is necessary to induced localized ballooning in the simulation.

The material and behavior models active in these VTB demonstration cases are tabulated in Table 4.1 and Table 4.2. The tables include the model name as identified in the BISON documentation [38], a brief description of what the model computes, and references for the model. These references can also be found on the BISON documentation page associated with each model.

4.2   Results

Standard fuel performance metrics were extracted from the examples to illustrate the expected behavior of the examples. The frictional and frictionless cases are compared against one another. Metrics of interest in this work include fuel centerline temperature, fission gas release, plenum

Table 4.1. Recommended UO$_2$ fuel models as used in the VTB examples.

Model Name	Brief Description	References
AxialRelocation	Computes the axial movement of fragmented fuel during a LOCA.	[27]
ComputeThermalExpansionEigenstrain	Computes thermal expansion given a constant instantaneous thermal expansion coefficient.	
Density	Computes evolving density due to volumetric changes. The initial density is supplied.	
HighBurnupStructureFormation	Determines the fraction of fuel that has restructured into the HBS.	[8]
UO2CreepUpdate	Computes thermal and irradiation creep of the fuel using a modified MAT-PRO correlation.	[5]
UO2Dispersal	Determines whether the fuel has dispersed. All fuel in locations where the cladding hoop strain is > 3 % are assumed to disperse.	[6]
UO2IsotropicDamageElasticityTensor	Computes the elastic properties of the fuel. Degradation assuming isotropic cracking is included.	[7]
UO2Pulverization	Determines whether the fuel has finely fragmented as a function of local temperature and burnup.	[50]
UO2RelocationEigenstrain	Computes an effective radial displacement that accounts for eccentricity and cracking effects.	[33]
UO2Sifgrs	Computes the evolution of gaseous fission products including production, diffusion, resolution, and release. Couples to volumetric swelling.	[7, 39]
UO2Thermal	Defines the thermal properties of UO$_2$. The recommended thermal conductivity model is NFIR. Corrections to the thermal conductivity in the HBS are captured using the KAMPF model.	[1, 29]
UO2VolumetricSwellingEigenstrain	Computes isotropic volume changes due to densification and solid and gaseous fission product swelling. Couples to fission gas behavior.	[5, 39]

Table 4.2. Recommended Zircaloy-4 cladding models as used in the VTB examples.

| Model Name	Brief Description	References
ZryCladdingFailure	Computes cladding failure during a LOCA given a specified criterion. The plastic instability criterion is used. Failure occurs when the inelastic strain rate exceeds 2.87×10^{-2} s^{-1}.	[34, 17]
ZryCreepLOCAUpdate	Computes thermal and irradiation creep in both the normal operating and LOCA regimes. The creep law is phase dependent, which is important during LOCA conditions.	[14, 17, 28]
ZryIrradiationGrowthEigenstrain	Computes the volume preserving axial growth for Zircaloy due to its anisotropic microstructure in the α-phase. To preserve volume diametrical shrinkage occurs.	[20]
ZryOxidation	Computes the oxide scale thickness and mass gain associated at both low and high temperatures.	[11, 32, 42]
ZrPhase	Computes the phase transformation of Zircaloy at high temperatures.	[37]
ZryThermal	Computes thermal properties for Zircaloy cladding as a function of temperature.	[5]
ZryThermalExpansionMATPROEigenstrain	Computes thermal expansion as a function of temperature and anisotropy.	[5]
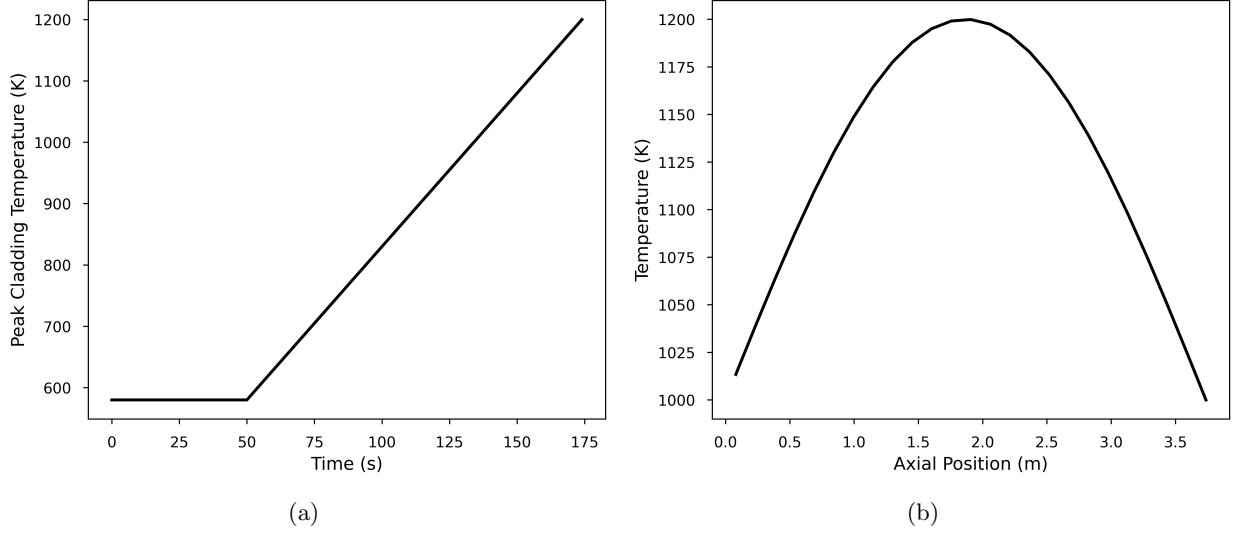
Figure 4.2. (a) Time evolution of the peak cladding temperature from the beginning of the LOCA and (b) the axial profile of the temperature once the peak of 1200 K is reached.

pressure, and fuel and cladding elongation for the normal operation. For the LOCA-like transient, metrics include the axial cladding profilometry, the time to rupture, and the mass dispersed.
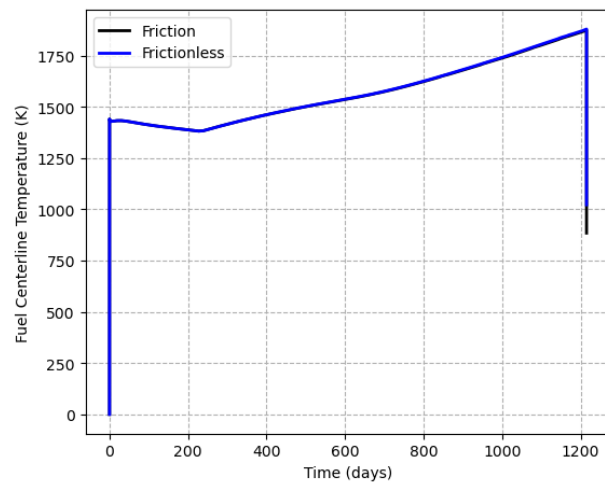
4.2.1 Normal Operation

The results for normal operation of the normal operation case are presented in Figure 4.3. As expected, fuel centerline temperature and fission gas release are unaffected by the inclusion of friction, whereas elongation and plenum pressure are strongly impacted. This was also observed in the improvements of some of the available validation cases for FFRD discussed in Section 3. Once contact is established, sticking between the fuel and cladding causes any further displacement to occur at the same rate (see Figure 4.3d). This behavior also results in the plenum volume remaining larger than in the frictionless case resulting in a lower rod internal pressure.

4.2.2 LOCA-like Transient

These VTB examples are still in the process of being developed, only the frictionless LOCA simulation is ready. The cladding profilometry for this example is plotted alongside the rod internal pressure evolution in Figure 4.4

Time to rupture for the case without friction is 124.41 s post-blowdown. The fuel mass dispersed assuming all fuel in axial regions where the cladding hoop strain has achieved 3% is 46.9 g.
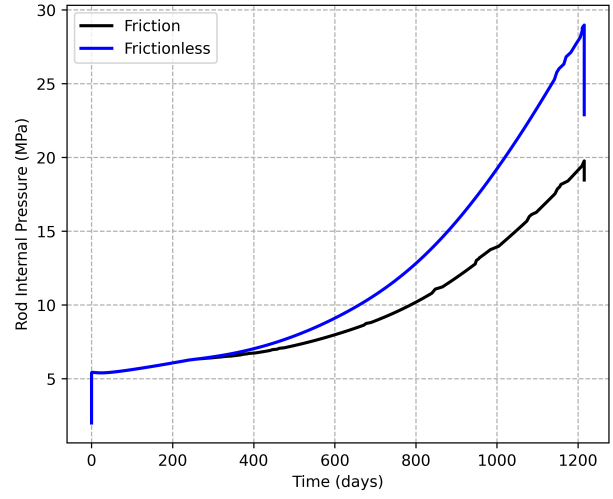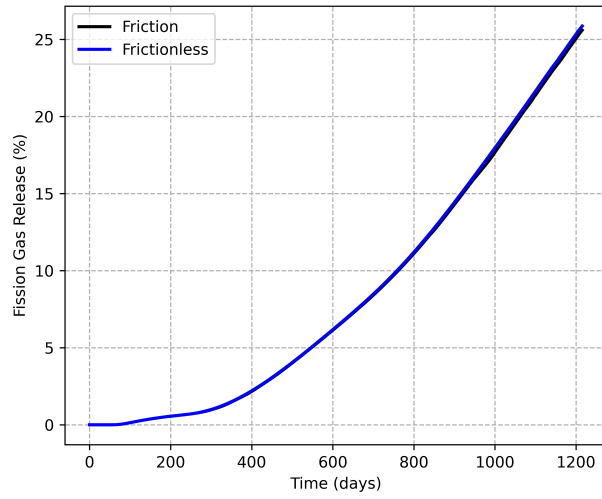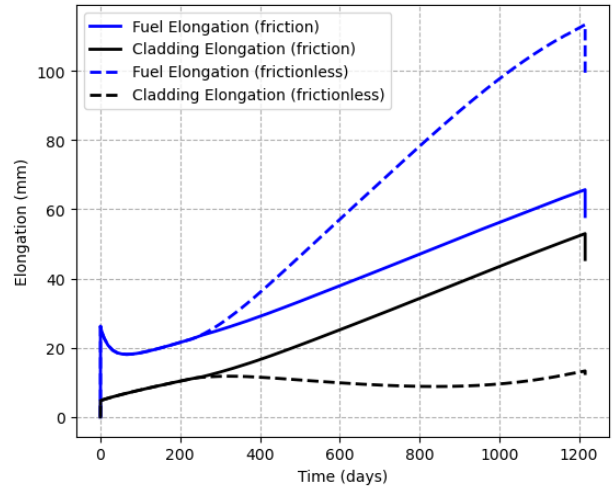
Figure 4.3. Results of the normal operation VTB example: (a) fuel centerline temperature, (b) plenum pressure, (c) fission gas release, (d) elongation.
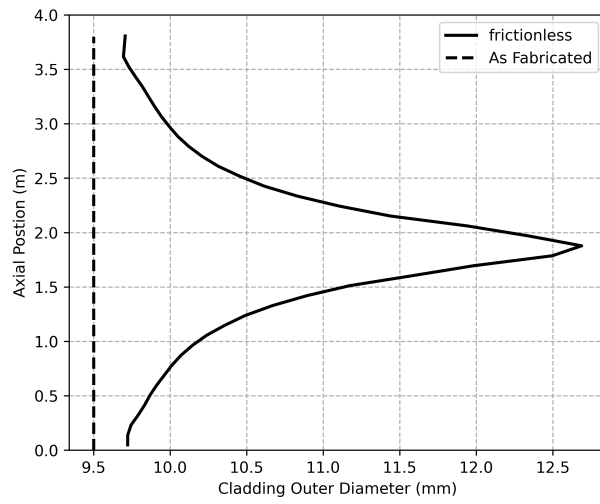
(a)
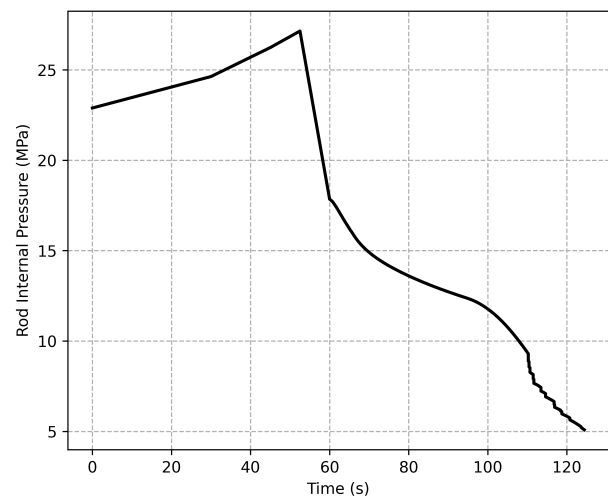
(b)

Figure 4.4. (a) Cladding diameter profile as a function of axial position and (b) plenum pressure evolution during the LOCA.

5. Models to Consider for Bayesian Calibration

Recently, the NEAMS program has invested in the development of Bayesian inference techniques in MOOSE's stochastic tools module [13]. These techniques can be used to gain an improved understanding of existing models given known experimental data. Bayesian techniques can be used to identify how much of the uncertainty in model predictions comes from the form of the model equations or the experimental data. These terms are commonly referred to as the model form and experimental uncertainty, respectively. Part of Dhulipala et al.'s [13] work involved applying the newly implemented techniques to the existing UO_2 creep model available in BISON. A key outcome of Bayesian calibration over simple linear regression typically employed in the creation of empirical correlations is that the coefficients in the equations are distributions themselves. Application of Bayesian calibration to the UO_2 creep model demonstrated an improvement in experimental predictions for the tribulation assessment cases available in BISON.

This section of the report is devoted to identifying models used in FFRD analysis that would benefit from Bayesian calibration going forward. Some of the underlying research to demonstrate the need for further model investigation has been funding under NEAMS and some by other funding sources. The models identified that most likely benefit from Bayesian calibration include the lower-length scale pulverization criterion, the empirical correlations for large fragment sizes, the HBS porosity correction used in thermal conductivity calculations, high-temperature cladding creep, transient fission gas release, and the fragment and pulver shape.

5.1 Lower-length Scale Pulverization Criterion

The work of Aagesen et al. [2, 3, 4] has resulted in a pulverization threshold that compares the bubble pressure in HBS bubbles to a critical bubble pressure. Pulverization occurs if the critical bubble pressure is exceeded. The correlations for critical bubble pressure (P_g^{cr}) were derived from phase-field fracture simulations on a singular bubble present in a HBS structure, subjected to a temperature ramping rate of 5 K/s. Several simulations were performed to determine the gas pressure in the bubble that initiated fracture of the HBS structure. The following equation for P_g^{cr} in Pa was fit to the 2D data [3]:

$$P_g^{cr} = 1.0 \times 10^6 \left[\left(124.17 + 1.43858 \left(\sigma_{gb}^{cr} - 130 \right) \right) (1 - p) - 1.0178 \sigma_H \right] \tag{5.1}$$

where σ_{gb}^{cr} and σ_H are in MPa. For the 3D data, the equation of P_g^{cr} in Pa becomes [4]:

$$P_g^{cr} = 1.0 \times 10^6 \left[\left(175.987 + 0.5035 \left(\sigma_{gb}^{cr} - 130 \right) \right) \left(1 - 1.582p \right) - 1.089\sigma_H \right] \tag{5.2}$$

where σ_H is the hydrostatic stress, p is the porosity, and σ_{gb}^{cr} is the critical fracture stress of the grain boundaries intersecting the bubble. The critical fracture stress of the grain boundaries is obtained from atomistic scale simulations. While the new pulverization thresholds utilized physics-informed models, the number of simulations and operational conditions are limited. Bayesian calibration would help identify whether a different functional form for P_g^{cr} would more accurately predict pulverization in separate effect and integral tests. Obtaining access to the NFIR and SCIP data would benefit this effort greatly.

5.2   Large Fragment Size Correlations

The large fragment size correlations were briefly mentioned in Section 2.2. The functional form of the equations were summarized by Gamble et al. [21]. Figure 5.1 and Figure 5.2 are reproduced from [21] illustrating the number of large fragments that form alongside available experimental data. Clearly, when considering burnup effects, the predicted number of fragments are far from the available data. Bayesian calibration could be used to explore different functional equations for the number of fragments, n_f, that form as a function of peak power and burnup. Accurately computing the number of fragments is important as it is directly used in computing the effective diameter of the large fragments, which in turn is used in dispersal and axial relocation calculations.
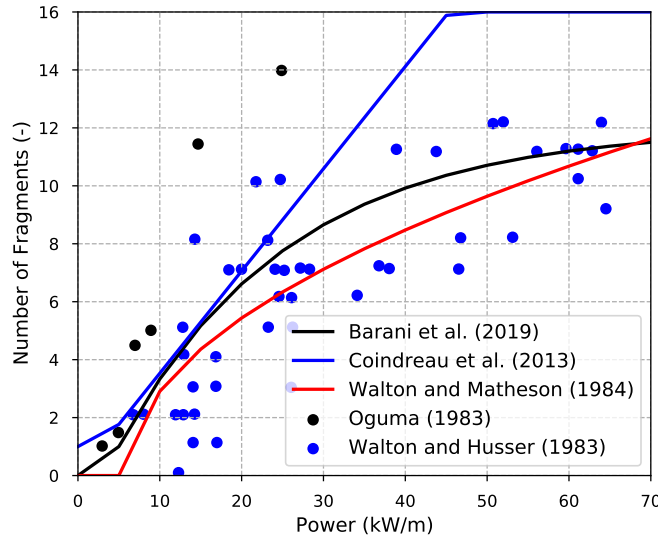

Figure 5.1. Comparisons between the three empirical correlations for predicting the number of radial fuel fragments for fresh fuel including experimental data from Walton and Husser [51].
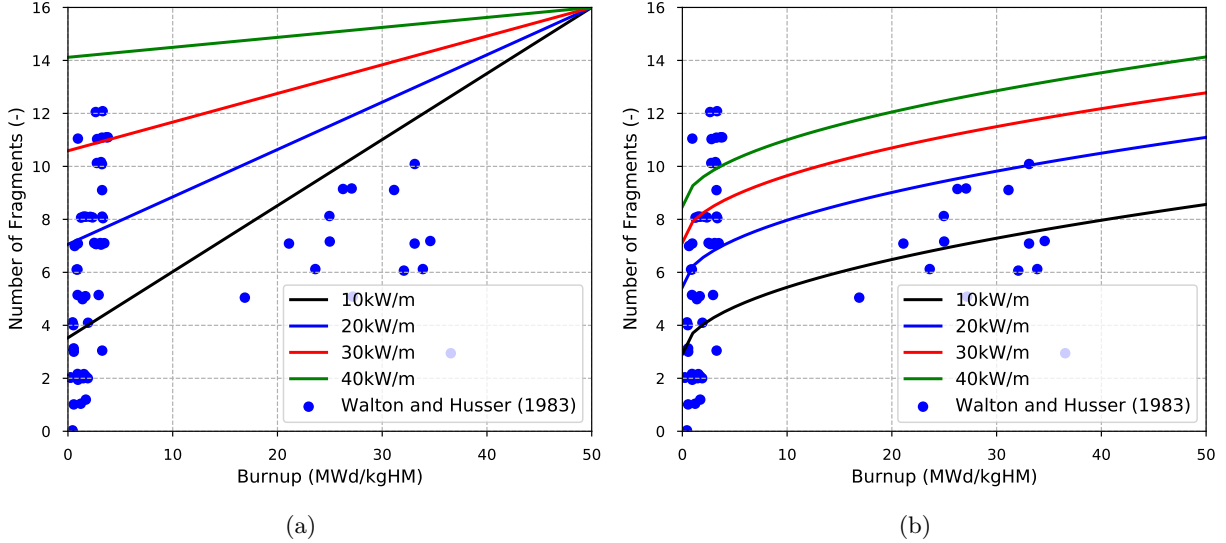
Figure 5.2. Increase in the number of radial fragments formed as a function of burnup for different maximum power levels for (a) the Coindreau et al. and (b) the Walton and Matheson models including experimental data from Walton and Husser [51].

5.3 High-burnup Structure Porosity Correction

When the HBS forms, the fuel restructures into a small grain highly porous medium. These pores tend to accumulate fission gases, which have poor thermal conductivities. Since the pores are larger than the grain structure, the local thermal conductivity of the fuel is expected to decrease. A model was added to BISON a few years ago that computes the porosity in the HBS and computes an effective thermal conductivity at the engineering scale that is weighted by the HBS volume fraction at a material point. This is used to weigh the contributions of the non-restructured fuel thermal conductivity and thermal conductivity in the HBS pores. Details of the methodologies for computing the effective thermal conductivity can be found in Toptan et al. [48]. Figure 5.3 presents the least squares fit currently employed in BISON for the HBS porosity. Couple this with the wealth of data and uncertainty associated with the thermal conductivity of UO_2 compiled by [48], and it becomes clear this is an area that would also benefit from Bayesian calibration.

5.4 High-temperature Cladding Creep

Many of the available assessment cases in BISON are separate effects cladding burst experiments. These cases provide a strong experimental foundation for assessing high-temperature creep correlations in BISON. The large strains obtained during ballooning are formed due to creep mechanisms. BISON currently has three high-temperature creep models available: Erbacher, Donaldson, and Kaddour. The details of these models are summarized in [23]. To date, in assessment cases, only the Erbacher model has been thoroughly tested since it is the first model available. All three
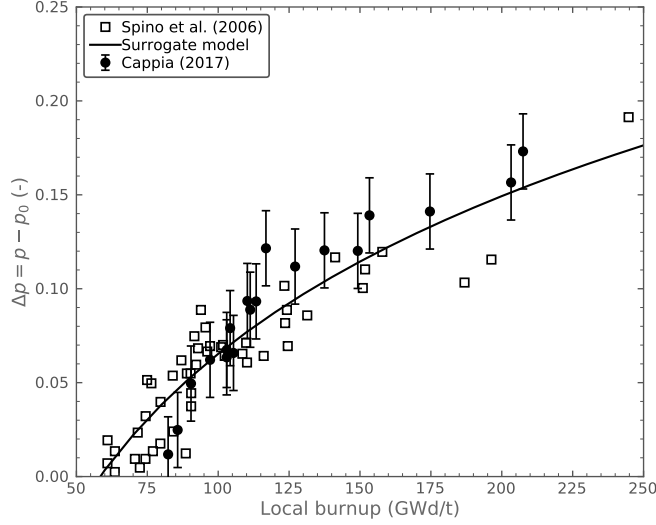
Figure 5.3. The porosity in the HBS as a function of burnup.

models follow a power law formulation, but the leading coefficients and activation energies differ and are a function of the Zircaloy-4 phase. It has been identified that BISON simulations using the Erbacher model for certain loading conditions (primarily at higher pressures and temperature ramp rates) yield unsatisfactory predictions. Given the importance of high temperature cladding creep to LOCA behavior, evaluation of these models and application Bayesian inference to identify where the uncertainty arises from is of great importance.

5.5 Transient Fission Gas Release

The NRC RIL [6] identified that understanding transient fission gas release (tFGR) is crucial to licensing of high-burnup fuel rods. Two models are currently available in BISON for predicting tFGR, an empirical one by Capps et al. [10] based upon three experiments and a mechanistic one presented in Aagesen et al. [4] coupled to pulverization. Both of these models have their limitations and have not been validated to experiments presented in the RIL that measure fission gas released during the LOCA. Much of the data highlighted in the RIL comes from SCIP and will be used for validation and calibration of the tFGR models once available.

The mechanistic model requires further development that could be explored in conjunction with Bayesian calibration. The current model determines the volume of gas released due to pulverization. Cube-shaped fragments whose bubbles intersect the free surface of a fragment upon pulverization release the quantity of gas in these bubbles. Further investigation into different particle shapes is required. There is also experimental evidence that tFGR may also result from microcracking of grains during the temperature rise. This is the basis of the empirical model by Capps et al. [10]. Effects of ramping rates need to also be explored. Bayesian calibration can be used to optimize the model form which may adopt a weight of the two models depending upon the conditions experienced

during the LOCA.

5.6   Fragment and Pulver Shape and Size

In Section 2.2, additional particle shapes for the binary system used in axial relocation calculations were presented. In terms of the packing fraction computed, the selection of particle shape was negligible. However, selection of particle size has a strong influence on the effective diameter of the particle used in dispersal calculations. Figure 5.4 presents the sieving data from Studsvik [18]. Additional data of this form is available for some of the Halden rods [46] and the fueled SATS tests [55]. This data combined with the ability to select the particle shape could be used with Bayesian calibration to develop and optimize a model that will introduce a distribution on both particle shape and size. It is envisioned that some pulvers could be octahedrons of a certain characteristic size, and others could be prismatic particles with a different characteristic size. This would not only improve dispersal calculations but also optimize the axial fuel relocation model.
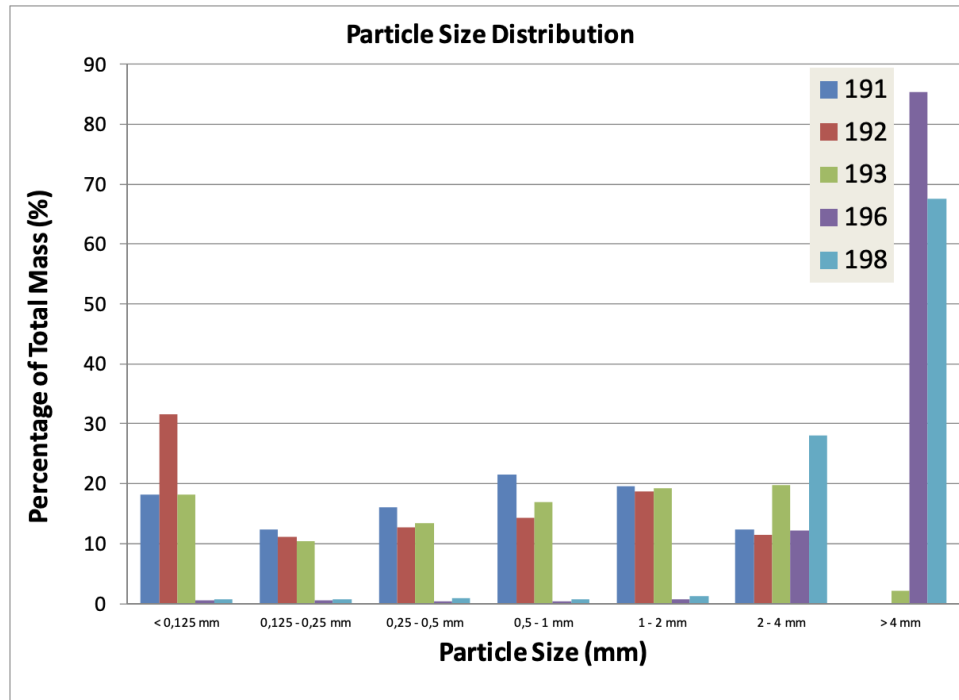

Figure 5.4. Particle distributions from the Studsvik Rods. Reproduced from [18].

6. Conclusions

Development of the FFRD and LOCA assessment database in BISON began in 2015. Since then additional empirical and LLS-informed models have been added to the cases to improve the code calculations in relation to the experimental data. Remaining gaps have been identified, and active work is ongoing to develop models in an attempt to understand the behavior of a high-burnup fuel rod during a LOCA.

In this report, new capabilities that have been added to BISON were described, including fuel dispersal, frictional contact in Layered1D simulations, and fragment and pulver shape selection. These models were applied to existing validation cases to evaluate their impact. It was found the selection of dispersal criterion identified in the NRC RIL had an impact when using the LLS-informed pulverization criterion. For short rodlets, the increased elongation and impact on the stress state during base irradiation offered by frictional contact had limited impact on fuel relocation ballooning and subsequent fuel relocation. This is due to the inherent limitation of Layered1D to describe multidirectional strain and stress states. The selection of the particle shape had limited impact on the effective packing fraction calculated, but the fragment and pulver equivalent diameters were strongly impacted.

An overview of the existing experimental data available in the BISON assessment suite was presented, with highlights of additional data that may be available if access to SCIP can be obtained. A discussion on missing data needs was also presented.

Last, models of importance in accurately predicting fuel rod behavior during a LOCA including FFRD that are ideal candidates for Bayesian calibration using new techniques added to MOOSE [13] are discussed. This approach has already been applied to the standard UO_2 creep model with an optimized model that yielded improved experimental comparisons. This section of the report is to be used as the basis for future work in improving the BISON predictions against the existing FFRD and LOCA database.

Bibliography

[1] A. Marion (NEI) letter dated June 13, 2006 to H. N. Berkow (USNRC/NRR). Safety Evaluation by the Office of Nuclear Reactor Regulation of Electric Power Research Institute (EPRI) Topical Report TR-1002865, "Topical Report on Reactivity Initiated Accidents: Bases for RIA Fuel rod Failures and Core Coolability Criteria". http://pbadupws.nrc.gov/docs/ML0616/ML061650107.pdf, 2006.

[2] L. Aagesen, S. Biswas, W. Jiang, A. Jokissari, S. Andersson, C. Matthews, and M. Cooper. Determine fragmentation criteria in high-burnup uo$_2$ fuel during accident conditions. Technical Report INL/EXT-20-00558 Rev. 0, Idaho National Laboratory, 2020.

[3] L. K. Aagesen, S. Biswas, W. Jiang, D. Andersson, M. Cooper, and C. Matthews. Mesoscale simulations to inform microstructure-based pulverization criterion in high-burnup UO$_2$. Technical Report INL/EXT-21-64275 Rev. 0, Idaho National Laboratory, 2021.

[4] L. K. Aagesen, S. Biswas, K. Gamble, W. Jiang, P.-C. Simon, and B. Spencer. Implementation and testing of physics-based pulverization model in BISONx. Technical Report INL/RPT-22-67941 Rev. 0, Idaho National Laboratory, 2022.

[5] C. M. Allison, G. A. Berna, R. Chambers, E. W. Coryell, K. L. Davis, D. L. Hagrman, D. T. Hagrman, N. L. Hampton, J. K. Hohorst, R. E. Mason, M. L. McComas, K. A. McNeil, R. L. Miller, C. S. Olsen, G. A. Reymann, and L. J. Siefken. SCDAP/RELAP5/MOD3.1 code manual, volume IV: MATPRO-A library of materials properties for light-water-reactor accident analysis. Technical Report NUREG/CR-6150, EGG-2720, Idaho National Engineering Laboratory, 1993.

[6] M. Bales, A. Chung, J. Corson, and L. Kyriazidis. Interpretation of Research on Fuel Fragmentation, Relocation, and Dispersal at High Burnup. Technical Report RIL 2021-13, United States Nuclear Regulatory Commission, 2021.

[7] T. Barani, A. Magni, D. Pizzocri, L. Cognini, P. Van Uffelen, L. Luzzi, and G. Pastore. Modeling and assessment of intra-granular bubble evolution and coarsening in uranium dioxide. In *NuMat18: The nuclear materials conference*, Seattle, USA, 2018.

[8] T. Barani, D. Pizzocri, F. Cappia, L. Luzzi, G. Pastore, and P. Van Uffelen. Modeling high burnup structure in oxide fuels for application to fuel performance codes. part

I: High burnup structure formation. *Journal of Nuclear Materials*, 539:152296, 2020. doi:10.1016/j.jnucmat.2020.152296.

[9] M. Billone, Y. Yan, T. Burtseva, and R. Daum. Cladding embrittlement during postulated loss-of-coolant accidents. Technical Report NUREG-6967, U.S. Nuclear Regulatory Commission, 2008.

[10] Nathan Capps, Larry Aagesen, David Andersson, Oliver Baldwin, W. Cade Brinkley, Michael W.D. Cooper, Jason Harp, Stephen Novascone, Pierre-Clément A. Simon, Christopher Matthews, and Brian D. Wirth. Empirical and mechanistic transient fission gas release model for high-burnup loca conditions. *Journal of Nuclear Materials*, 584:154557, 2023. ISSN 0022-3115. doi:https://doi.org/10.1016/j.jnucmat.2023.154557. URL `https://www.sciencedirect.com/science/article/pii/S0022311523003240`.

[11] J. V. Cathcart, R. E. Pawel, R. A. McKee, R. E. Druschel, G. J. Yurek, J. J. Campbell, and S. H. Jury. Zirconium metal-water oxidation kinetics, IV. reaction rate studies. Technical Report ORNL/NUREG-17, Oak Ridge National Laboratory, 1977.

[12] O. Coindreau, F. Fichot, and J. Fleurot. Nuclear fuel rod fragmentation under accidental conditions. *Nuclear Engineering and Design*, 255:68–76, 2013.

[13] S. L. N. Dhulipala, D. Schwen, Y. Che, R. Sweet, A. Toptan, Z. Prince, P. German, and S. Novascone. Massively parallel bayesian model calibration and uncertainty quantification with applications to nuclear fuels and materials. Technical Report INL/RPT-23-73383 Rev. 0, Idaho National Laboratory, 2022.

[14] A.T. Donaldson, T. Healey, and R.A.L. Horwood. Biaxial creep deformation of zircaloy-4 pwr fuel cladding in the alpha,(alpha + beta) and beta phase temperature ranges. Technical report, British Nuclear Energy Society, 1985.

[15] Bole du Chomont F. LOCA Testing at Halden; The Ninth Experiment IFA-650.9. Technical Report HWR-917, OECD Halden Reactor Project, 2009.

[16] M. Ek. LOCA Testing at Halden; The Second Experiment IFA-650.2. Technical Report HWR-813, OECD Halden Reactor Project, 2005.

[17] F. J. Erbacher, H. J. Neitzel, H. Rosinger, H. Schmidt, and K. Wiehr. Burst criterion of Zircaloy fuel claddings in a loss-of-coolant accident. In *Zirconium in the Nuclear Industry, Fifth Conference, ASTM STP 754, D.G. Franklin Ed.*, pages 271–283. American Society for Testing and Materials, 1982.

[18] M. Flanagan, B. C. Oberländer, and A. Puranen. Fuel fragmentation, relocation and dispersal under loca conditions: Experimental observations. In *Proceedings of TopFuel2013*, 2013.

[19] M. E. Flanagan, P. Askeljung, and A. Puranen. Evaluation of mechanistic and empirical models against existing ffrd and loca experimental databases. Technical Report NUREG-2160, United States Nuclear Regulatory Commission, 2013.

[20] DG Franklin. Zircaloy-4 cladding deformation during power reactor irradiation. In *Zirconium in the Nuclear Industry*. ASTM International, 1982.

[21] K. A. Gamble, T. W. Knight, E. Roberts, J. D. Hales, and B. W. Spencer. Mechanistic verification of empirical uo$_2$ fuel fracture models. *Journal of Nuclear Materials*, 556:153163, 2021. doi:10.1016/j.jnucmat.2021.153163.

[22] K. A. Gamble, L. K. Aagesen, S. Biswas, W. Jiang, A. Martin Recuero, J. D. Hales, D. Van Wasshenova, M. W. D. Cooper, N. Capps, and R. Sweet. Advancements in modeling fuel pulverization and cladding behavior during a LOCA. Technical Report INL/EXT-21-64705 Rev. 1, Idaho National Laboratory, 2022.

[23] K. A. Gamble, R. T. Sweet, P.-C. A. Simon, L. K. Aagesen, and S. Biswas. Evaluation of mechanistic and empirical models against existing ffrd and loca experimental databases. Technical Report INL/RPT-22-69625 Rev. 0, Idaho National Laboratory, 2022.

[24] G. L. Giudicelli, A. Abou-Jaoude, A. J. Novak, A. Abdelhameed, P. Balestra, L. Charlot, J. Fang, B. Feng, T. Folk, R. Freile, T. Freyman, D. Gaston, L. Harbour, T. Hua, W. Jiang, N. Martin, Y. Miao, J. Miller, I. Naupa, D. O'Grady, D. Reger, E. Shemon, N. Stauff, M. Tano, S. Terlizzi, S. Walker, and C. Permann. The virtual test bed (VTB) repository: A library of reference reactor models using NEAMS tools. *Nuclear Science and Engineering*, 0(0):1–17, 2023. doi:10.1080/00295639.2022.2142440.

[25] D.G. Hardy. High Temperature Expansion and Rupture Behaviour of Zircaloy Tubing. In *CSNI Proceeding of the Specialist Meeting on Safety of Water Reactor Fuel Elements in Saclay*, Saclay, France, October 22-24 1973.

[26] M. Helin and J. Flygare. NRC LOCA tests at Studsvik, design and construction of test train device and tests with unirradiated cladding material. Technical Report STUDSVIK/N-11/130, Studsvik, 2012.

[27] L. O. Jernkvist and A. Massih. Models for axial relocation of fragmented and pulverized fuel pellets in distending fuel rods and its effects on fuel rod heat load. Technical Report 2015:37, Quantum Technologies AB, 2015.

[28] D. Kaddour, S. Frechinet, A.F. Gourgues, J.C. Brachet, L. Portier, and A. Pineau. Experimental determination of creep properties of zirconium alloys together with phase transformation. *Scripta Materialia*, 51(6):515–519, 2004.

[29] H Kämpf and G Karsten. Effects of different types of void volumes on the radial temperature distribution of fuel pins. *Nuclear Technology*, 9(3):288–300, 1970. doi:10.13182/NT70-A28783.

[30] L. Kekkonen. LOCA Testing at Halden; The Fourth Experiment IFA-650.4. Technical Report HWR-838, OECD Halden Reactor Project, 2007.

[31] A. Lavoil. LOCA Testing at Halden; The Tenth Experiment IFA-650.10. Technical Report HWR-974, OECD Halden Reactor Project, 2010.

[32] S. Leistikow, G. Schanz, H. v. Berg, and A.E. Aly. Comprehensive presentation of extended Zircaloy-4/steam oxidation results 600-1600 C. In *CSNI/IAEA specialists meeting on water reactor fuel safety and fission product release in off-normal and accident conditions*, Riso Nat. Lab., Denmark, 1983.

[33] Eds. M. A. Kramman, H. R. Freeburn. Escore–the epri steady-state core reload evaluator code: General description. Technical Report EPRI NP-5100, Electric Power Research Institute, February 1987.

[34] V. Di Marcello, A. Schubert, J. van de Laar, and P. Van Uffelen. The TRANSURANUS mechanical model for large strain analysis. *Nuclear Engineering and Design*, 276:19–29, 2014.

[35] M. E. Markiewicz and F.J. Erbacher. Experiments on ballooning in pressurized and transiently heated Zircaloy-4 tubes. Technical Report KfK 4343, Kernforschungszentrum Karlsruhe GmbH (Germany), Kernforschungszentrum Karlsruhe, Germany, 1988.

[36] Caleb P. Massey, Kurt A. Terrani, Sebastien N. Dryepondt, and Bruce A. Pint. Cladding burst behavior of Fe-based alloys under LOCA. *Journal of Nuclear Materials*, 470:128–138, 2016. ISSN 0022-3115. doi:http://dx.doi.org/10.1016/j.jnucmat.2015.12.018. URL http://www.sciencedirect.com/science/article/pii/S0022311515303871.

[37] A.R. Massih. Transformation kinetics of zirconium alloys under non-isothermal conditions. *Journal of Nuclear Materials*, 384:330–335, 2009.

[38] Computational Mechanics and Materials Department Idaho National Laboratory. Bison: A finite element-based nuclear fuel performance code. https://mooseframework.inl.gov/bison/syntax/index.html.

[39] G. Pastore, L. Luzzi, V. Di Marcello, and P. Van Uffelen. Physics-based modelling of fission gas swelling and release in UO_2 applied to integral fuel rod analysis. *Nuclear Engineering and Design*, 256:75–86, 2013.

[40] Erzsébet Perez-Feró, Csaba Győri, Lajos Matus, László Vasáros, Zoltán Hózer, Péter Windberg, László Maróti, Márta Horváth, Imre Nagy, Anna Pintér-Csordás, and Tamás Novotny. Experimental database of e110 claddings exposed to accident conditions. *Journal of Nuclear Materials*, 397(1):48–54, 2010. ISSN 0022-3115. doi:https://doi.org/10.1016/j.jnucmat.2009.12.005. URL https://www.sciencedirect.com/science/article/pii/S0022311509009271.

[41] S. A. Pitts, S. R. Novascone, H. Chen, B. W. Spencer, S. Satpathy, R. J. Gardner, and J. D. Hales. Verify and validate 1.5d capability. Technical Report CASL-U-2017-1380-000, Consortium for Advanced Simulation of LWRs, 2017.

[42] J. T. Prater and E. L. Courtright. Zircaloy-4 oxidation at 1300 to 2400 C. Technical Report NUREG/CR-4889, PNL-6166, Pacific Northwest Lab, 1987.

[43] P. Raynaud and I. Porter. Predictions of fuel dispersal during a LOCA. In *Proceedings of WRFPM 2014*, 2014.

[44] A. Recuero, D. Yushu, and D. Schwen. Interface problem formulation improvements with application to nuclear fuel performance analysis. Technical Report INL/RPT-23-74423 Rev. 0, Idaho National Laboratory, 2023.

[45] M. A. Snead, Y. Yan, M.l Howell, J. R. Keiser, and K. A. Terrani. Severe Accident Test Station design document. Technical report, Oak Ridge National Laboratory, 9 2015. URL `https://www.osti.gov/biblio/1252142`.

[46] H. Sonnenburg, W. Wiesenack, J. Karlsson, J. Noirot, V. Garat, N. Waeckel, F. Khattout, A. Cabrera-Salcedo, J. Zhang, G. Khvostov, A. Gorzel, V. Brankov, F. Nagase, P. Raynaud, M. Bales, T. Taurines, T. Nakajima, and A. Alvestav. Report on fuel fragmentation, relocation, and dispersal. Technical Report NEA/CSNI/R(2016)16, Organisation for Economic Co-operation and Development, Nuclear Energy Agency, Committee on the Safety of Nuclear Installations, 2016.

[47] J. Stuckert, M. Grosse, M. Steinbrueck, M. Walter, and A. Wensauer. Results of the QUENCH-LOCA experimental program at KIT. *Journal of Nuclear Materials*, 534:152143, 2020. ISSN 0022-3115. doi:https://doi.org/10.1016/j.jnucmat.2020.152143. URL `https://www.sciencedirect.com/science/article/pii/S0022311519315971`.

[48] A. Toptan and K. A. Gamble. Bison high burnup structure modeling capabilities validated with a selection of the halden ifa-650 rods. Technical Report INL/EXT-20-60778, Idaho National Laboratory, 2020.

[49] R. Tradotti. LOCA Testing at Halden, The BWR Fuel Experiment IFA-650.14. Technical Report HWR-1084, OECD Halden Reactor Project, 2014.

[50] J. A. Turnbull, S. K. Yagnik, M. Hirai, D. M. Staicu, and C. T. Walker. An assessment of the fuel pulverization threshold during loca-type temperature transients. *Nuclear Science and Engineering*, 179:477–485, 2015.

[51] L. A. Walton and D. L. Husser. Fuel pellet fracture and relocation. In *IAEA Specialists Meeting on Water Reactor Fuel Element Performance Computer Modelling*, 1983.

[52] L. A. Walton and J. E. Matheson. FUMAC - a new model for light water reactor fuel relocation and pellet-cladding interaction. *Nuclear Technology*, 64:127–138, 1984.

[53] R. L. Williamson, K. A. Gamble, D. M. Perez, S. R. Novascone, G. Pastore, R. J. Gardner, J. D. Hales, W. Liu, and A. Mai. Validating the BISON fuel performance code to LWR experiments. *Journal of Nuclear Materials*, 301:232–244, 2016.

[54] R. L. Williamson, J. D. Hales, S. R. Novascone, G. Pastore, K. A. Gamble, B. W. Spencer, W. Jiang, S. A. Pitts, A. Casagranda, D. Schwen, et al. BISON: A flexible code for advanced

simulation of the performance of multiple nuclear fuel forms. *Nuclear Technology*, 207(7): 954–980, 2021. doi:10.1080/00295450.2020.1836940.

[55] Y. Yan, Z. Burns, T. Smith, K. D. Linton, K. Yueh, and K. A. Terrani. LOCA fragmentation test with high burnup HBR fuel rod. Technical Report ORNL/TM-2019/1239, Oak Ridge National Laboratory, 2019.